Design Procedure for a Digital Proportional-Resonant Current Controller in a Grid Connected Inverter

Tiago Davi Curi Busarello
Department of Engineering
Federal University of Santa Catarina
Blumenau, Brazil
tiago.busarello@ufsc.br

José Antenor Pomilio
School of Electrical and Computer Engineering
University of Campinas
Campinas, Brazil
antenor@fee.unicamp.br

Marcelo Godoy Simões
Department of Electrical Engineering and Computer Science
Colorado School of Mines
Golden, USA
msimoes@mines.edu

***Abstract*— This paper presents a design procedure for a digital Proportional-Resonant (PR) current controller in a Grid Connected Inverter (GCI). The procedure describes a systematic list of how to compute the proportional and resonant gains as well as the coefficients for the digital resonant path. The main contribution of the design procedure is to facilitate and to support researchers who are designing GCI with current control strategies in a digital environment. The paper also presents a frequency domain analysis of a designed digital PR controller. The fictitious *w*-domain is used in such analysis. A case study shows the efficacy of GCI with a digital PR current controller designed based on the proposed procedure. Later, the paper discusses that the proposed procedure is valid also for digital PR controller with multiple resonant paths.**

Keywords—current control; DC-AC power converters; inverters; notch filters; proportional-resonant controller.

I. INTRODUCTION

DC-AC converters with output filter are a dominant and an indispensable technology for connecting Renewable Energy Sources (RES) to the electric grid. The converter allows energy transaction between the RES and the grid in a suited, safety and reliable manner. Such kind of DC-AC converter is familiarly known as Grid Connected Inverters (GCI) or even Grid-tied Inverters.

GCIs are controlled in voltage or current mode. The current-controlled GCI is an attractive choice because its operation is not strongly dependent on the grid impedance as occurs in voltage-controlled GCI [1]. Additionally, a GCI with the current controller can offer overcurrent protection without additional effort.

A boundless number of control strategies have been developed with employing current controller for single-phase GCI. Some of the most common is the modified PI [2], [3], lead-lag [4], dead-beat [5], repetitive [6], [7] and Proportional-Resonant (PR) controller [8]–[12], each one with its features, advantages, and drawbacks.

The PR controller is gaining special attention due to its simplicity and modularity. Once the PR controller is defined as a proportional gain added to a resonant path tuned at a frequency of interest, other resonant paths are easily added to the PR controller without the need to redesign the original controller.

Indeed, GCI with PR controller is commonly found in the literature. Some of them describe the procedure to design the PR controller [13]–[15]. All of these researches have their legitimacy, and they show the PR efficacy. However, most of them describe their procedure presenting the PR controller in continuous-time style while the majority of GCI applications involves digital implementation. In this case, it falls to the reader the burden to find out how to employ the PR controller digitally.

In this context, this paper presents a design procedure for a digital PR current controller applied to a GCI. The procedure describes a step-by-step method to compute the proportional and resonant gains, as well the coefficients for the resonant path. The main contribution is to facilitate and to support researchers who are designing GCI with current control strategies in a digital environment. The paper also presents a frequency domain analysis of a digital PR controller. The fictitious *w*-domain is used in such analysis. A case study shows the efficacy of GCI with a digital PR current controller designed using the proposed procedure. Later, the paper discusses that the proposed procedure is valid also for multiple resonant path PR controllers.

II. SYSTEM DESCRIPTION

Fig. 1 presents a single-phase GCI as well as the block diagram of the control strategy. The inverter is connected to the grid through an inductor (L). R_{inv} represents the inductor winding resistance. The grid is represented by the sinusoidal voltage source and by a line impedance (R_g and L_g). The inverter output current and the grid voltage are sensed, and the measured signals are sent to the control block.

The research presented in this paper is sponsored by National Council for Scientific and Technological Development – CNPq (grants 421281/2016-2 302257/2015-2) and São Paulo Research Foundation – FAPESP (grant 2016/08645-9).

978-1-5386-8257- 9/18/$31.00 ©2018 IEEE

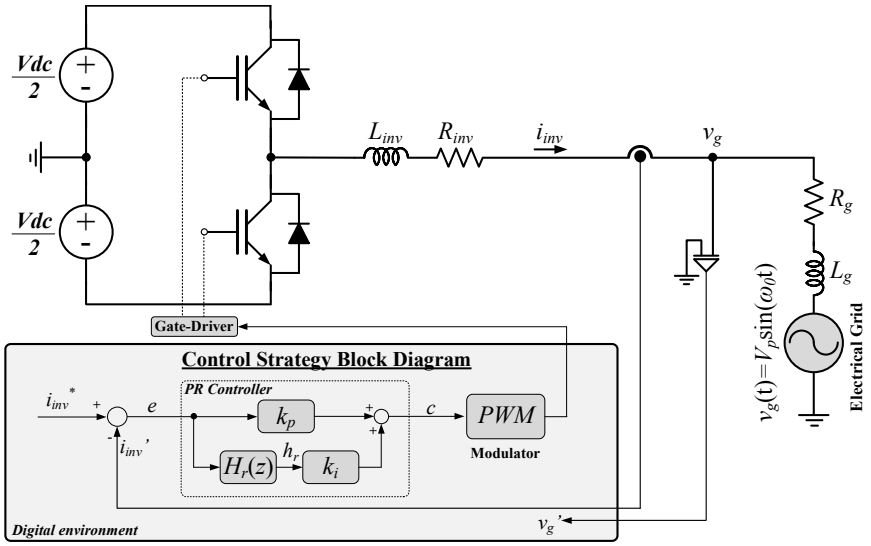

Fig. 1. Single-phase GCI as well as the block diagram of the control strategy

The inverter output current is compared to the reference signal, resulting in the error signal which passes through the digital PR controller. The PR output signal acts in the inverter via a PWM modulator. The modulator has a carrier with amplitude equals one. The reference is a sinusoidal signal synchronized with the grid voltage, that's the reason why the voltage is sensed and sent to the diagram. The synchronization is guaranteed by a Phase-Locked Loop [16] not shown in this figure. The time constant of the current control loop is much longer than the time delay of the PWM. Therefore, the delay caused by the PWM can be neglected without compromising the current controller design [17].

III. Design Procedure for the Digital PR Controller

The digital PR controller in Fig. 1 consists of a proportional gain (k_p) added to a resonant path. The resonant path consists of the resonant gain (k_i) and the resonant filter, which is described by a z-domain transfer function $H_r(z)$ and it is given by (1).

$$H_r(z) = \frac{b_0 + b_1 z^{-1} + b_2 z^{-2}}{a_0 + a_1 z^{-1} + a_2 z^{-2}} \quad (1)$$

Where b_k and a_k are real constants.

The resonant filter is also known as *Notch Filter*. Throughout this paper, the term resonant filter will be used. Therefore, the design of a digital PR controller falls in obtaining the values of k_p, k_i, a_0, a_1, a_2, b_0, b_1, and b_2. The design procedure presented in this section is valid for the half-bridge inverter shown in Fig. 1. However, this procedure is also valid for the full-bridge inverter and three-phase inverter. For the three-phase inverter, it is enough to replicate the designed PR controller to the other phases.

A. 1st step: knowing the system parameters

The first step to design a digital PR controller is to know, or to define, the system parameter. Tab. I shows the parameters, System Parameters their label and their units that the designer must know beforehand. The variable names are those shown in Fig. 1.

TABLE I. System Paramenters

Parameter	Variable	Unit
Inverter Output Filter Inductance	L_{inv}	H
Inverter Output Filter Resistance	R_{inv}	Ω
Total Inverter DC-Link Voltage	V_{dc}	V
Switching Frequency	f_{sw}	Hz
Current Sensor Gain	H_i	A/A
Inverter Nominal Power	P_{inv}	W
Sampling Frequency	f_a	Hz
Sampling Angular Freqency	$\omega_a = 2\pi f_a$	rad/s
Sampling Period	$T_a = 1/f_a$	s
Peak Voltage of the Grid	V_p	V
Grid Frequency	f_g	Hz
Grid Angular Frequency	$\omega_g = 2\pi f_g$	rad/s

2sd step: defining the desired PR parameters

Tab. II shows the parameters that must be defined as well as their variable and units. The most important parameter to define is the resonant frequency, which is the frequency in which the controller will act to reach zero steady-state error.

B. 3rd step: computing the proportional and resonant gains

The proportional (k_p) and the resonant (k_i) gains of the PR controller are calculated according to (2) and (3) [18], respectively. Notice that the resonant angular frequency appears in the equations and the total DC-link voltage is divided by two due to the inverter half-bridge topology.

TABLE II. DERSIRED PR PARAMETERS

Parameter	Variable	Unit
Resonant Frequency	f_r	Hz
Resonant Angular Frequency	$\omega_r = 2\pi f_r$	rad/s
Resonant Bandwidth	B_s	Hz
Resonant Angular Bandwidth	$B_r = 2\pi B_s$	rad/s
Damping Factor	ξ	-

$$k_p = \frac{(2\xi+1)\sqrt{(2\xi+1)}\omega_r L_{inv} - R_{inv}}{\frac{V_{dc}}{2}} \frac{1}{H_i} \quad (2)$$

$$k_i = \frac{\omega_r^2 L_{inv}\left[(2\xi+1)^2 - 1\right]}{2\frac{V_{dc}}{2}} \frac{1}{H_i} \quad (3)$$

C. 4th step: computing the resonant filter constants

The fourth step consists in computing the coefficients a_0, a_1, a_2, b_0, b_1 and b_2 of the z-domain transfer function. These coefficients can be obtained by applying the Z-transform into the transfer function of an s-domain analog resonant filter, given by

$$H_{r\_ana\log}(s) = \frac{k_r B_r s}{s^2 + 2B_r s + \omega_r^2} \quad (4)$$

Where k_r is the resonant gain.

Applying the Z-transform through Backward-Euler approximation [19] in (4) results in the digital resonant filter, given by

$$H_r(z) = \mathbb{Z}\left\{H_{r\_ana\log}(s)\right\} = \frac{b_0 + b_1 z^{-1} + b_2 z^{-2}}{a_0 + a_1 z^{-1} + a_2 z^{-2}} \quad (5)$$

Thus, the coefficients of the resonant filter are given by the following expressions:

$$b_0 = k_r B_r T_a \quad (6)$$

$$b_1 = \left[-k_r B_r e^{-0.5 B_r T_a} \cos\left(T_a\sqrt{\omega_r^2 - 0.25 B_r^2}\right) - C\right] T_a \quad (7)$$

Where C is a constant defined by

$$C = \frac{0.5 k_r B_r^2}{\sqrt{\omega_r^2 - 0.25 B_r^2}} e^{-0.5 B_r T_a} \sin\left(T_a\sqrt{\omega_r^2 - 0.25 B_r^2}\right) \quad (8)$$

$$b_2 = 0 \quad (9)$$

$$a_0 = 1 \quad (10)$$

$$a_1 = -2e^{-0.5 B_r T_a} \cos\left(T_a\sqrt{\omega_r^2 - 0.25 B_r^2}\right) \quad (11)$$

$$a_2 = e^{-B_r T_a} \quad (12)$$

Notice that the a_0 is intentionally defined as 1 to allow writing the z-domain transfer function shown in (1) as a difference equation given by

$$\begin{aligned} y(n) &= b_0 u(n) + b_1 u(n-1) + b_2 u(n-2) \\ &\quad -\left[a_1 y(n-1) + a_2 y(n-2)\right] \end{aligned} \quad (13)$$

Where $y(n)$ and $x(n)$ are the output and input of the resonant filter, respectively. This step is one of the main contribution of this paper. It allows the designer to compute the coefficients of the resonant filter only by defining the desired frequency response of a filter in s-domain. Later, equations (6) to (12) give the coefficients for digital implementation.

IV. CASE STUDY

A case study is conducted to design a digital PR current controller using the procedure mentioned above and to implement it in a GCI as shown in Fig. 1. Tab. III presents the parameters. The resonant gain for the analog filter k_r was chosen to one because the resonant gain of the digital PR controller is computed separately by (3) and implemented separately as shown in Fig. 1. Tab. IV presents the parameters for the designed digital PR controller. All values obtained must have at least twelve decimal places for better accuracy.

TABLE III. PARAMETERS VALUES IN THE CASE STUDY

Parameter	Variable	Value
Total Inverter DC-Link Voltage	V_{dc}	450 V
Inverter Output Filter Resistance	R_{inv}	0.5 mΩ
Inverter Output Filter Inductance	L_{inv}	10 mH
Switching Frequency	f_{sw}	30 kHz
Current Sensor Gain	H_i	0.1 A/A
Inverter Nominal Power	P_{inv}	1500 W
Sampling Frequency	f_a	30 kHz
Sampling Angular Freqency	$\omega_a = 2\pi f_a$	1.88x10^5 rad/s
Sampling Period	$T_a = 1/f_a$	33.333 µs
Peak Voltage of the Grid	V_p	180 V
Grid Frequency	f_g	60 Hz
Grid Angular Frequency	$\omega_g = 2\pi f_g$	377 rad/s
Grid inductance	L_g	100 uH
Grid resistance	R_g	0.1 mΩ
Resonant Frequency	f_r	60 Hz
Resonant Angular Frequency	$\omega_r = 2\pi f_r$	377 rad/s
Resonant Bandwidth	B_s	1.5 Hz
Resonant Angular Bandwidth	$B_r = 2\pi B_s$	10.053 rad/s
Damping Factor	ξ	0.95
Resonant Gain for the Analog Filter	k_r	1

TABLE IV. DESGNED DIGTAL PR CONTROLLER

Parameter	Variable	Value
Proportional Gain	k_p	0.827435088694
Resonant Gain	k_i	234.028059558631
B0 coefficient	b_0	$3.14159265359x10^{-4}$
B1 coefficient	b_1	$-3.141344635858x10^{-4}$
B2 coefficient	b_2	0
A0 coefficient	a_0	1
A1 coeffiecient	a_1	-1.999528003287
A2 coefficient	a_2	0.999685890077

To numerically verify the accuracy of the design PR controller and its frequency response, the case study uses the fictitious *w*-domain [19] with a fictitious *w*-plane. The *w*-domain is a tool that allows analyzing systems in *z*-domain through frequency charts similar to those found in *s*-domain. All features found in the frequency domain is valid for the *z*-plane mapped into *w*-plane, except for high frequencies. The transformation from *z*-plane to *w*-plane occurs by applying the *w*-transformation given by

$$z = \frac{1+\left(T_a/2\right)w}{1-\left(T_a/2\right)w} \tag{14}$$

The frequency of the *w*-plane is related to the frequency of the *s*-plane through the following relationship

$$v = \frac{2}{T_a}\tan\frac{\omega T_a}{2} \tag{15}$$

Where v and ω are the frequency in *w* and *s* planes, respectively.

The resonant filter of the PR controller, described by $H_r(z)$, is initially analyzed. Therefore, the designed resonant filter is mapped into the *w*-plane according to

$$H_r(w) = H_r(z)\Big|_{z=\frac{1+\left(T_a/2\right)w}{1-\left(T_a/2\right)w}} \tag{16}$$

Once the designed resonant filter is in *w*-plane, the magnitude and argument functions are given by (17) and (18), respectively.

$$Mag_{Hr}(v) = 20\log\left|H_r(w)\right| \tag{17}$$

$$Phase_{Hr}(v) = \arg\left[H_r(w)\right] \tag{18}$$

Fig. 2 presents the magnitude response in *w*-domain of the designed resonant filter. Only at 60 Hz the gain is equal to 0 dB, showing the efficacy of the designed resonant filter. This chart shows that only the component at 60 Hz of the error is multiplied by one. All other components are attenuated considerably. Notice that the resonant filter does not include

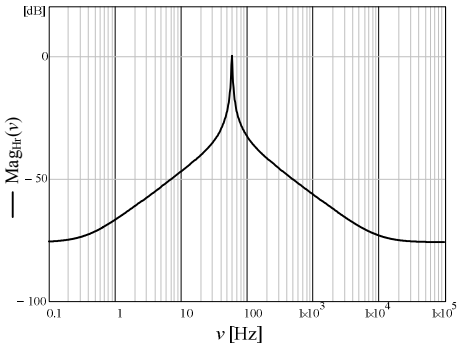

Fig. 2. Magnitude response in *w*-domain of the designed resonant filter.

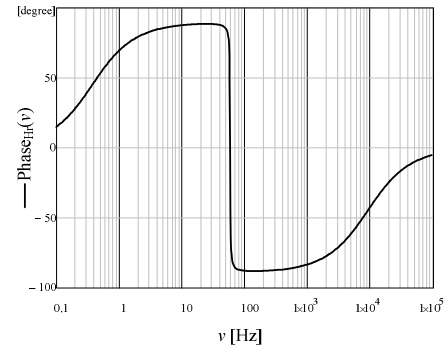

Fig. 3. Phase response in *w*-domain of the designed resonant filter.

the resonant gain computed in the third step of the design procedure.

Fig. 3 presents the phase response in *w*-plane of the resonant filter. The phase suffers a 180 degrees shift at the resonance due to the poles of the transfer function.

The transfer function, which describes the PR controller, is given by

$$TF_{PR}(z) = k_p + k_i H_r(z) = k_p + k_i\frac{b_0 + b_1 z^{-1} + b_2 z^{-2}}{a_0 + a_1 z^{-1} + a_2 z^{-2}} \tag{19}$$

Similarly, the *z*-domain PR controller transfer function can be mapped into the *w*-domain. Thus, the PR controller transfer function is given by

$$TF_{PR}(w) = TF_{PR}(z)\Big|_{z=\frac{1+\left(T_a/2\right)w}{1-\left(T_a/2\right)w}} \tag{20}$$

The magnitude and argument functions are given by (21) and (22), respectively.

$$Mag_{TFPR}(v) = 20\log\left|TF_{PR}(w)\right| \tag{21}$$

$$Phase_{TFPR}(v) = \arg\left[TF_{PR}(w)\right] \tag{22}$$

Fig. 4 presents the magnitude response of the designed PR controller. The highest amplification occurs at 60 Hz. The gain at this frequency is equal to 47.414 dB corresponding closely to the computed resonant gain.

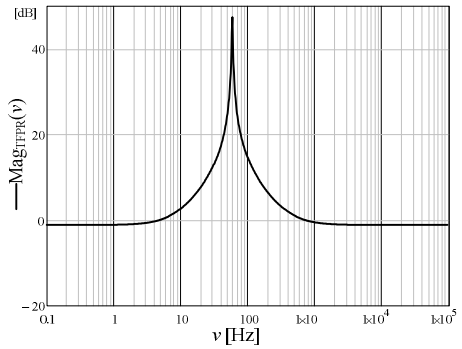

Fig. 4. The magnitude response of the designed PR controller.

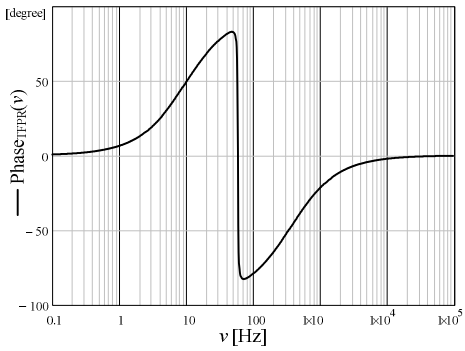

Fig. 5. The phase response of the designed PR controller.

Fig. 5 presents the phase response of the designed PR controller. The phase is zero for low and high frequencies, and it suffers the same phase-shift found in the resonant filter.

Fig. 6 presents the inverter output current (i_{inv}) and its reference signal reference (i_{inv}*) during a step from the null current to a sinusoidal waveform. The PR controller makes the output current to follow its reference with negligible steady-state error, as will be plotted later. During the transient period, the PR controller responds rapidly and does not make the inverter output current to present highly oscillatory behavior.

Fig. 7 presents inverter output current (i_{inv}) and its reference (i_{inv}*) during a reference step-up, as well as a zoom during the transient. Similar to the previous case, the PR controller responds slightly fast and without making a high oscillatory behavior in the inverter output current. Similar behavior is obtained for a step-down reference change.

Fig. 8 presents the inverter output current (i_{inv}) and its reference (i_{inv}*) during a step from sinusoidal waveform to a null reference. The PR controller makes the inverter output current to reach null current in a few milliseconds.

Fig. 9 presents the error (e) and resonant filter output (hr) signals in steady-state condition. The error signal is noisily, and it contains a high harmonic content. The presence of harmonics is mainly due to the PWM and non-modeled elements. The y-axis of the error signal presents low values, indicating that the error is negligible.

The resonant filter output (hr) is a pure sinusoidal waveform at 60 Hz, indicating the efficacy of the designed resonant filter.

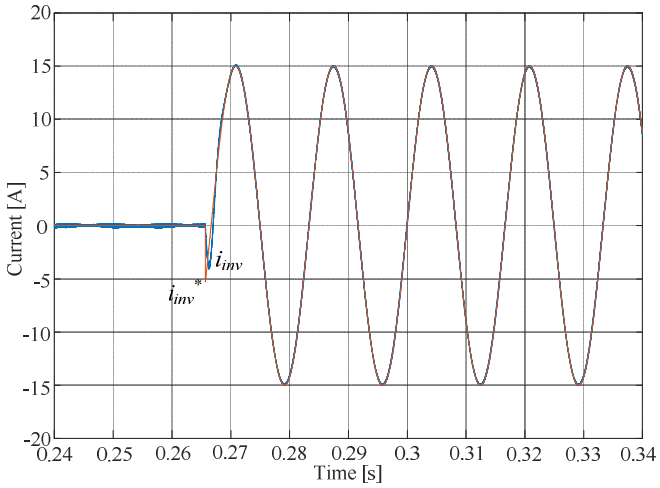

Fig. 6. Inverter output current (i_{inv}) and its signal reference (i_{inv}*) during a step from null current to a sinusoidal waveform.

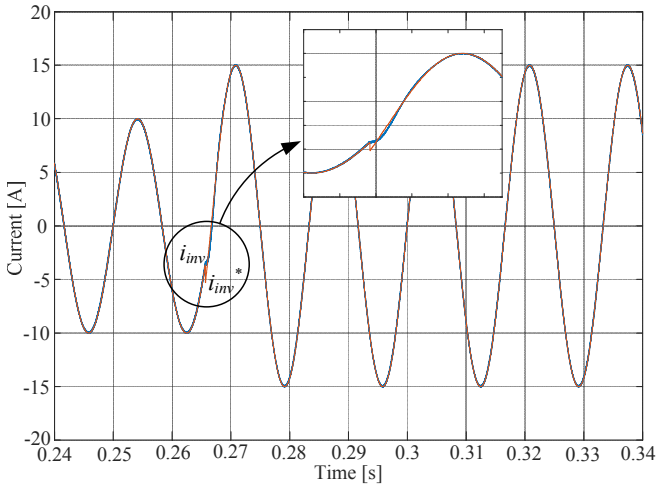

Fig. 7. Inverter output current (i_{inv}) and its signal reference (i_{inv}*) during a reference step-up as well as a zoom during the transient.

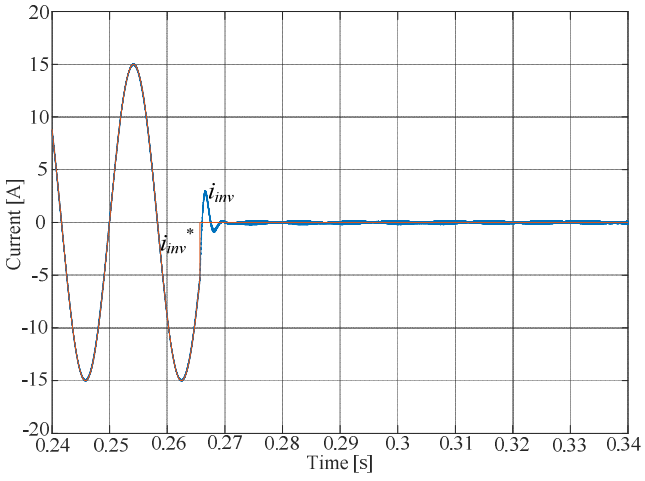

Fig. 8. Inverter output current (i_{inv}) and its signal reference (i_{inv}*) during a step from sinusoidal waveform to a null reference.

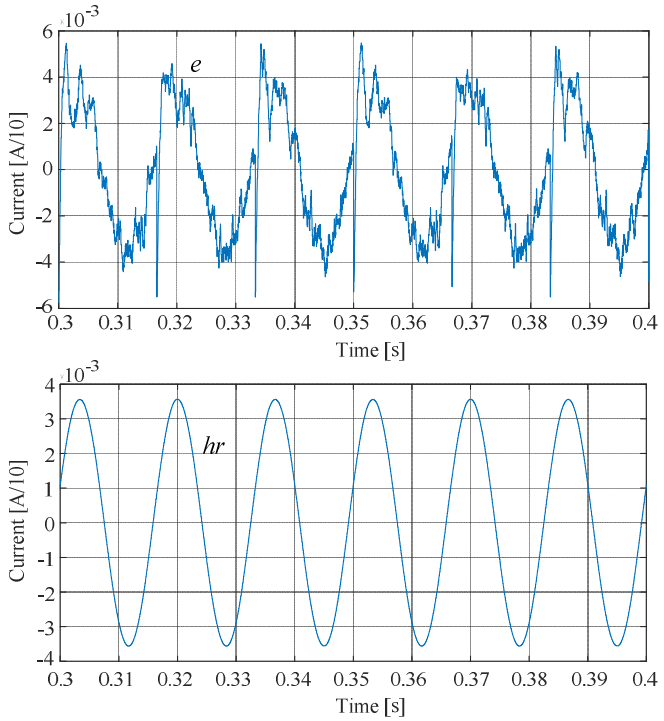

Fig. 9. The error (*e*) and resonant filter output (*hr*) signals during a steady-state condition

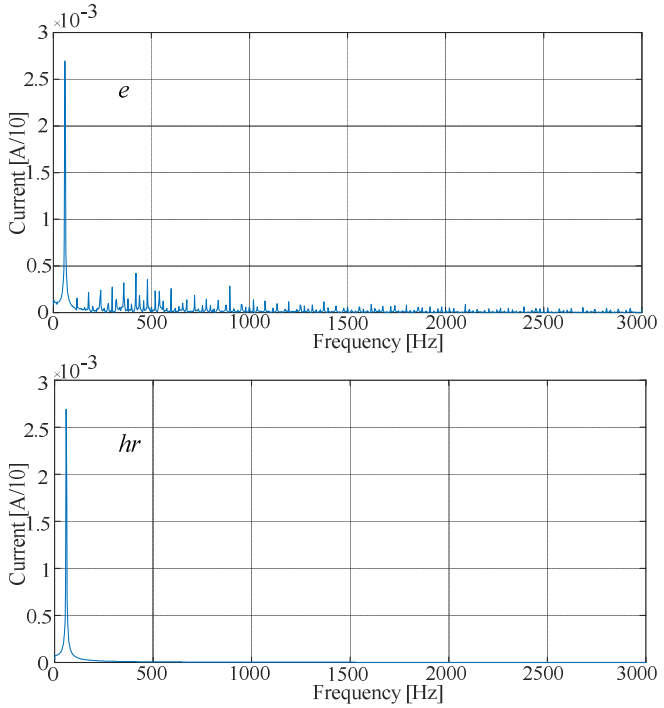

Fig. 10. The harmonic content of the error (*e*) and resonant filter output (*hr*) signals.

It is important to highlight that, and according to Fig. 1, the error is the input signal of the resonant filter. Therefore, the resonant filter is extracting only the 60 Hz component of the error signal, as showed in Fig. 10. The Total Harmonic

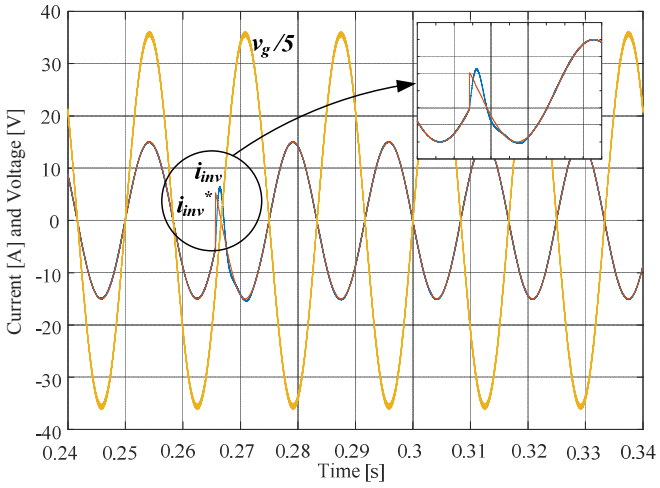

Fig. 11. The inverter output current (i_{inv}), its signal reference (i_{inv}*) and the grid voltage (v_g divided by 5) during a 180-degree reference change.

Distortion (THD) of the error signal is 40.7% while the THD of the resonant filter output signal is 0.4%. The THDs were calculated in 20 cycles with 60 Hz fixed-frequency and 30 kHz as the sampling frequency. The resonant output signal is later amplified by the designed resonant gain (k_i).

Fig. 11 presents the inverter output current (i_{inv}), its reference (i_{inv}*) and the grid voltage (v_g divided by 5) during a 180-degree reference change. A zoom during the change is also presented. The PR controller makes the inverter output current to follow its reference with negligible steady-state error, indicating that the design procedure is valid for a GCI injecting or draining current from the grid, knowing that the GCI DC source can receive energy. The synchronization is also observed in this result.

Fig. 12 presents the output signal of the PR controller output signal (*c*) and the error signal (*e*) during the 180-degree reference change. The main point to be highlighted here is that the PR controller output signal is always lower than one. Since the PWM has carrier amplitude equals one, the designed PR controller does not reach saturation during steady-state and transient periods.

V. Discussion

The procedure for designing a digital PR current controller is applied when the reference signal of the inverter output current is a sinusoidal waveform at a frequency of interest. Thus, the PR controller acts at such a frequency, ensuring negligible steady-state error in the controlled variable. However, it is common to use a reference signal that is created by summing two or more sinusoidal waveforms each one with its frequency. An example is a GCI that works as a Multifunctional Renewable Energy Device (RED) [20]–[22]. These devices perform their basic function, which is to transfer energy from the primary DC source to the grid and inject harmonic currents to act as an active filter. In this case, the reference signal is the sum of the fundamental component and some harmonic components, like the 3rd, 5th and 7th. Therefore, the PR current controller must

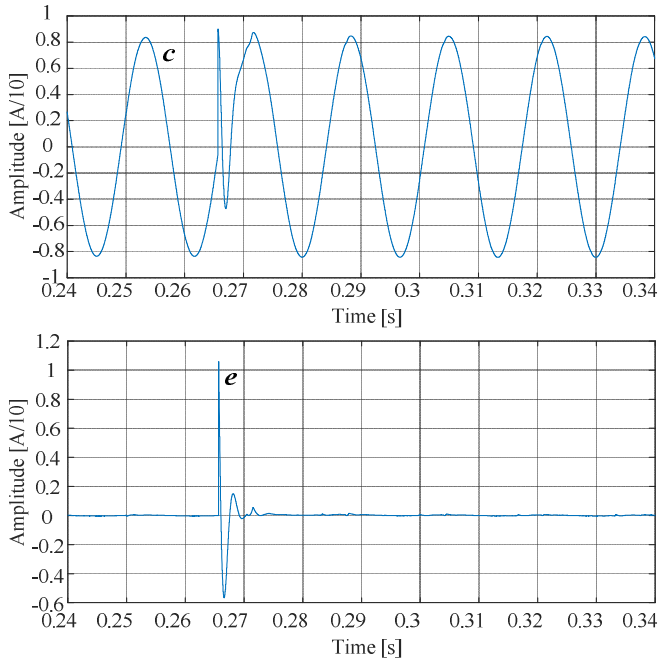

Fig. 12. The output signal of the PR controller (c), and the error signal (e) during the 180-degree reference change.

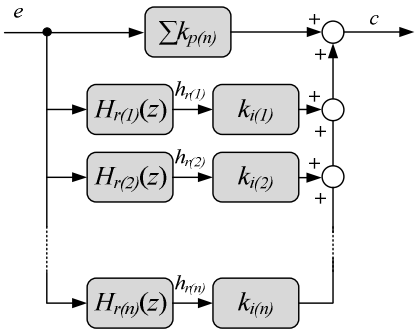

Fig. 13. PR current controller with n-resonant paths.

assure zero steady-state error in these components. To do that, additional resonant paths are designed. Even though the design procedure considers a single-frequency reference, it is easily expanded for a reference signal having more than one frequency.

Fig. 13 shows a PR current controller with n-resonant paths, each one with its resonant frequency and gain. To use the design procedure for multiple resonant paths, it's enough to perform the procedure individually for each resonant frequency of interest. Since (2) and (3) compute the PR proportional and resonant gains taking into account the resonant frequency, the proportional gain for PR with multiple paths must be summed. This is the reason why Fig. 13 shows the summation of proportional gains.

For the sake of illustration, the design procedure was computed individually for 60 Hz, and 300 Hz and the results were combined, forming a structure similar to that of Fig. 13. Fig. 14 presents the magnitude response of the designed combined resonant paths. The resonant frequencies of 60 and

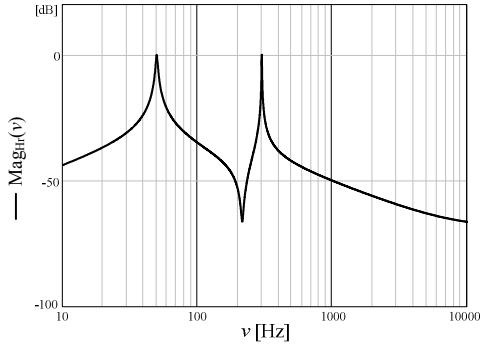

Fig. 14. The magnitude response of the designed combined resonant paths.

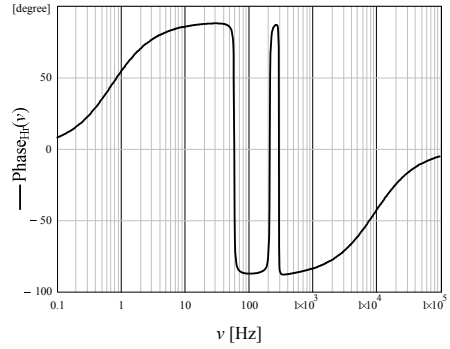

Fig. 15. The phase response of the designed combined resonant paths.

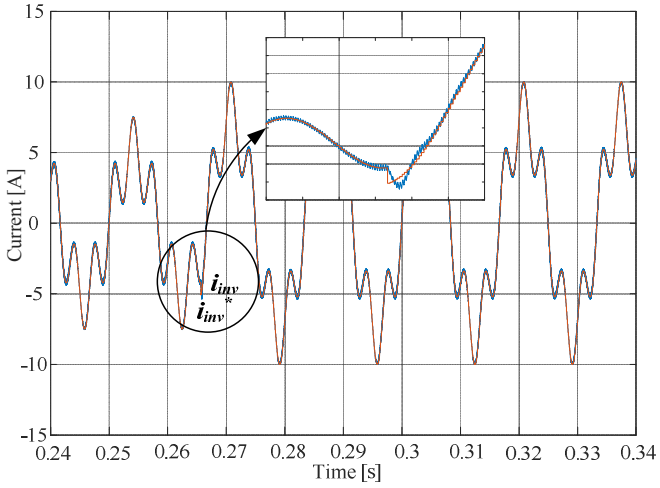

Fig. 16. Inverter output current (i_{inv}) and its signal reference (i_{inv}*) during a reference step-up

300 Hz are those that the gain is unity or close to it.

Fig. 15 presents the phase response of the designed combined resonant paths where the resonant frequencies are 60 Hz and 300 Hz. It occurs two 180-degree phase shift, one at 60 Hz and another at 300 Hz.

Fig. 16 presents the inverter output current (i_{inv}) and its reference (i_{inv}*) during a reference step-up, as well as a zoom during the transient. The reference signal is the sum of two

sinusoidal waveforms, one at 60 Hz and the other at 300 Hz and amplitude equals do 0 dB. The inverter output current follows its reference with a negligible steady-state error. The transient does not present an abnormal situation. Therefore, the digital PR controller with two resonant paths designed computing individually the procedure has shown an efficient result.

Another concern of employing PR controller is frequency detuning. This happens when the grid voltage suffers variation on the value of its fundamental frequency. At a first glance, the PR controller would not be able to make the output current to follow the signal reference with negligible steady-state error. However, due to the bandwidth of the PR controller, it can operate in frequencies around the tuned frequency with satisfactory response. The PLL also plays an important role in assuring that the reference keeps synchronized with the new value of the grid fundamental frequency. A simulation has been performed with fundamental frequency at 59.5 Hz. The results did not present meaningful differences over those of Section IV.

CONCLUSIONS

This paper presented a design procedure for a digital PR current controller in a GCI. The procedure consisted of a systematic list of how to compute the proportional and resonant gains as well the coefficients for the digital resonant path. After designing a PR current controller based on the proposed procedure, the paper presented a frequency domain analysis in the fictitious *w*-domain, showing that the proposed procedure is satisfactory for GCI in current-controlled mode. A case study as well as a discussion demonstrated the efficacy of the design procedure, making it an attractive tool for practical engineering. A prototype is under development to verify the proposed design procedure experimentally. Experimental results will be presented in a future opportunity. The simulation files used in this paper will be freely available on the author's webpage http://busarello.prof.ufsc.br.

REFERENCES

[1] M. H. J. Bollen e F. Hassan, Integration of Distributed Generation in the Power System. John Wiley & Sons, 2011.

[2] D. Shetty e N. Prabhu, "Ziegler Nichols method based Robust reactive current controller for STATCOM", Energy Procedia, vol. 117, p. 543–550, jun. 2017.

[3] M. T. Faiz, M. M. Khan, X. Jianming, S. Habib, e H. Tang, "Parallel feedforward compensation based active damping of LCL-type grid connected inverter", in 2018 IEEE International Conference on Industrial Technology (ICIT), 2018, p. 788–793.

[4] Y. S. Kuo, J. Y. Lin, J. C. Tang, e J. G. Hsieh, "Lead-lag compensator design based on vector margin and steady-state error of the step response via particle swarm optimization", in 2016 International Conference on Fuzzy Theory and Its Applications (iFuzzy), 2016, p. 1–6.

[5] L. Wang, N. Ertugrul, e M. Kolhe, "Evaluation of dead beat current controllers for grid connected converters", in IEEE PES Innovative Smart Grid Technologies, 2012, p. 1–7.

[6] J. N. da Silva, A. J. S. Filho, D. A. Fernandes, A. P. N. Tahim, E. R. C. da Silva, e F. F. Costa, "A discrete repetitive current controller for single-phase grid-connected inverters", in 2017 Brazilian Power Electronics Conference (COBEP), 2017, p. 1–6.

[7] K. Zhou, F. Blaabjerg, D. Wang, e Y. Yang, Periodic Control of Power Electronic Converters. Institution of Engineering and Technology, 2016.

[8] D. Zammit, C. Spiteri Staines, M. Apap, e J. Licari, "Design of PR current control with selective harmonic compensators using Matlab", J. Electr. Syst. Inf. Technol., vol. 4, no 3, p. 347–358, dez. 2017.

[9] S. Silwal e M. Karimi-Ghartemani, "On the design of proportional resonant controllers for single-phase grid-connected inverters", in 2016 12th IEEE International Conference on Control and Automation (ICCA), 2016, p. 797–803.

[10] H. Cha, T. K. Vu, e J. E. Kim, "Design and control of Proportional-Resonant controller based Photovoltaic power conditioning system", in 2009 IEEE Energy Conversion Congress and Exposition, 2009, p. 2198–2205.

[11] H. Khalfalla, S. Ethni, M. Al-Greer, V. Pickert, M. Armstrong, e V. T. Phan, "An adaptive proportional resonant controller for single phase PV grid connected inverter based on band-pass filter technique", in 2017 11th IEEE International Conference on Compatibility, Power Electronics and Power Engineering (CPE-POWERENG), 2017, p. 436–441.

[12] N. Kumar, T. K. Saha, e J. Dey, "Control, implementation, and analysis of a dual two-level photovoltaic inverter based on modified proportional resonant controller", IET Renew. Power Gener., vol. 12, no 5, p. 598–604, 2018.

[13] M. Castilla, J. Miret, J. Matas, L. G. de Vicuna, e J. M. Guerrero, "Control Design Guidelines for Single-Phase Grid-Connected Photovoltaic Inverters With Damped Resonant Harmonic Compensators", IEEE Trans. Ind. Electron., vol. 56, no 11, p. 4492–4501, nov. 2009.

[14] R. Teodorescu, F. Blaabjerg, M. Liserre, e P. C. Loh, "Proportional-resonant controllers and filters for grid-connected voltage-source converters", IEE Proc. - Electr. Power Appl., vol. 153, no 5, p. 750–762, set. 2006.

[15] N. Zhang, H. Tang, e C. Yao, "A Systematic Method for Designing a PR Controller and Active Damping of the LCL Filter for Single-Phase Grid-Connected PV Inverters", Energies, vol. 7, no 6, p. 3934–3954, jun. 2014.

[16] M. Karimi-Ghartema, Enhanced Phase-Locked Loop Structures for Power and Energy Applications. John Wiley & Sons, 2014.

[17] R. Teodorescu, M. Liserre, e P. Rodriguez, Grid Converters for Photovoltaic and Wind Power Systems. John Wiley & Sons, 2011.

[18] S. Bacha, I. Munteanu, e A. I. Bratcu, Power Electronic Converters Modeling and Control: with Case Studies. Springer Science & Business Media, 2013.

[19] K. Ogata, Discrete-time Control Systems. Prentice-Hall International, 1995.

[20] M. G. Simões, T. D. C. Busarello, A. S. Bubshait, F. Harirchi, J. A. Pomilio, e F. Blaabjerg, "Interactive smart battery storage for a PV and wind hybrid energy management control based on conservative power theory", Int. J. Control, vol. 89, no 4, p. 850–870, abr. 2016.

[21] T. D. C. Busarello e J. A. Pomilio, "Bidirectional multilevel shunt compensator with simultaneous functionalities based on the conservative power theory for battery-based storages", Transm. Distrib. IET Gener., vol. 9, no 12, p. 1361–1368, 2015.

[22] T. D. C. Buasarello e J. A. Pomilio, "Battery storage system with active filtering function based on the conservative power theory for wind generators", in 2018 IEEE International Conference on Industrial Electronics for Sustainable Energy Systems (IESES), 2018, p. 21–26.